Steel and Composite Structures, *Vol. 33, No. 3 (2019) 375-388*
DOI: https://doi.org/10.12989/scs.2019.33.3.375

Influence of slenderness on axially loaded square tubed steel-reinforced concrete columns

Biao Yan [1a], Dan Gan [*2], Xuhong Zhou [2b] and Weiqing Zhu [1c]

[1] *School of Highway, Chang'an University, Xi'an 710064, China*
[2] *Key Laboratory of New Technology for Construction of Cities in Mountain Area (Chongqing University), Ministry of Education, Chongqing 400045, China*

(*Received January 7, 2019, Revised May 17, 2019, Accepted October 18, 2019*)

Abstract. This paper aims to investigate the axial load behavior and stability strength of square tubed steel-reinforced concrete (TSRC) columns. Unlike concrete filled steel tubular (CFST) column, the outer steel tube of a TSRC column is mainly used to provide confinement to the core concrete. Ten specimens were tested under axial compression, and the main test variables included length-to-width ratio (L/B) of the specimens, width-to-thickness ratio (B/t) of the steel tubes, and with or without stud shear connectors on the steel sections. The failure mode, ultimate strength and load-tube stress response of each specimen were summarized and analyzed. The test results indicated that the axial load carried by square tube due to friction and bond of the interface increased with the increase of L/B ratio, while the confinement effect of tube was just the opposite. Parametric studies were performed through ABAQUS based on the test results, and the feasibility of current design codes has also been examined. Finally, a method for calculating the ultimate strength of this composite column was proposed, in which the slenderness effect on the tube confinement was considered.

Keywords: steel-reinforced concrete; square tubed column; axial load; column curve; design method

1. Introduction

A steel-reinforced concrete (SRC) column combines the advantages of both steel and concrete materials. Compared with a steel column, the fire resistance and durability of a SRC column are enhanced since the steel section is protected within concrete, local buckling of the steel section can be avoided, and the overall buckling strength of the column can be enhanced (Ellobody *et al*. 2011, Ky *et al*. 2015), "Compared with a concrete column, the shear resistance and ductility of a SRC column are improved (Kim *et al*. 2011), "However, to ensure the co-working performance of concrete and steel section, a reinforcement cage is needed (Zhu *et al*. 2017), usually leading to complicated beam-column connections (Fig. 1(a)).

To reduce the complexity of beam-column connection in SRC frame, as shown in Fig. 1, tubed SRC (TSRC) column was proposed by Zhou and Liu (2010), "The TSRC column is a kind of special SRC column in which the reinforcement cage in conventional SRC column is replaced by the outer thin-walled steel tube. Similar but different from concrete-filled steel tubular (CFST) columns (Chen *et al*. 2018, Liu *et al*. 2017), the outer steel tube of a TSRC column is mainly to confine the concrete core, not to directly resist the axial load. The outer thin-walled steel tube is terminated at the ends of the columns (i.e., the gaps at the column ends allow no external load is directly applied on the steel tube), "Compared with a SRC column, the confinement from the outer steel tube of a TSRC column to the concrete core is more effective, and concrete cover spalling when subjected to fire or earthquakes can also be restrained. Furthermore, the tube acting as both formwork and stirrups make concreting convenient. Circular TSRC columns have been successfully applied in a high-rise building in Chongqing, China (Fig. 1(c)).

The research about tubed concrete column was firstly conducted by Gardner and Jacobson (1967), "In the research, the stub columns were loaded in compression under the following end conditions to investigate the end effects on CFST columns: steel tube only loaded, concrete core only loaded, and both tube and concrete loaded. The second condition is a rudiment of tubed concrete column. In practice, to resist tensile force or flexural moment, reinforcement cages or steel sections are needed, and they were named as tubed RC (TRC) column (a reinforcement cage is arranged in the column) and tubed SRC (TSRC) column (a steel section is arranged in the column), respectively.

The TRC columns were primarily used to strengthen RC structures by Tomii *et al*. (1985), "The test results indicated that the outer steel tubes could significantly improve the shear strength, ductility, and absorption capacity of RC columns. Following this, the TSRC column was proposed by Zhou and Liu (2010) to simplify the construction procedure of SRC columns. Up to now, a series of tests on

*Corresponding author, Associate Professor, E-mail: gandan@cqu.edu.cn
[a] Ph.D., E-mail: yanb@chd.edu.cn
[b] Professor, E-mail: zhouxuhong@126.com
[c] Associate Professor, E-mail: zhuweiqing87@126.com

ISSN: 1229-9367 (Print), 1598-6233 (Online)

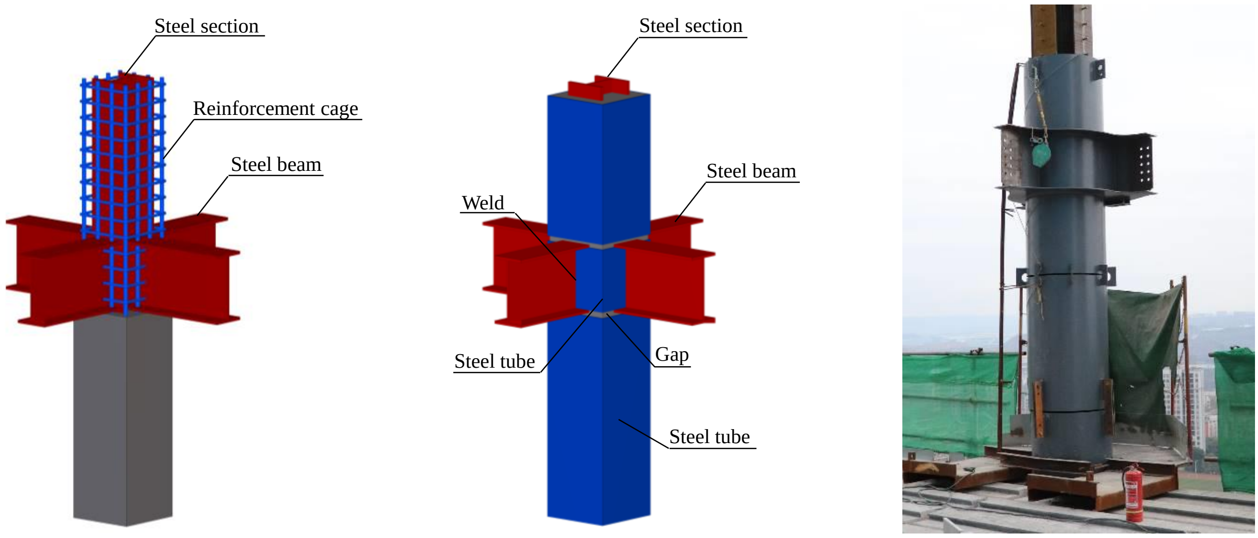

(a) SRC column (b) TSRC column (c) TSRC column in building

Fig. 1 Comparison of SRC and tubed SRC column

TSRC columns have been performed by the research group in Chongqing University, and the main conclusions are summarized as follows:

- For the short columns under axial compression, the tube confinement on concrete core increases the ultimate strength and ductility of concrete, which results in that the TSRC columns exhibit higher axial load capacity than that of the SRC columns with the same volumetric steel ratio (Qi *et al*. 2011).
- For the short columns under eccentric compression, the average confinement of steel tube is close to that of the columns under axial compression, and it is acceptable to assume that the stress-strain relationship of different concrete fibers is uniform when analyzing the eccentrically loaded short TSRC columns (Wang *et al*. 2016).
- For the short columns subjected to combined constant axial compression and lateral cyclic load, the shear strength, plastic deformation capacity, ductility index, and energy dissipating capacity of TSRC short columns were much higher than those of SRC columns with the same steel ratio and axial compressive load (Zhou and Liu 2010).

Previous studies have focused on the behavior of TSRC short columns. The performance of slender square TSRC columns is also worthy of concern, since the high load-bearing capacity of TSRC column may lead to a relatively smaller cross-section (Keo *et al*. 2015), "Compared with circular TSRC columns, the tube confinement of square TSRC columns is not pronounced. But considering the convenience in connecting the beams and walls, and the requirements of function or architectural layout, the square TSRC columns show more application potentials. Therefore, experimental investigations on square TSRC columns with different slenderness ratios are necessary and urgent. The main objective of this paper is to investigate the stability strength and ductility of square TSRC columns subjected to axial load, and a total of ten specimens were tested. Based on the calibration of test results, parametric studies were performed through ABAQUS. The feasibility of existing design codes has been verified through test and finite element (FE) analysis results. Moreover, a method for estimating the ultimate strength of square TSRC columns, in which taking the slenderness effect on tube confinement into account, was proposed based on large amounts of FE data.

2. Experimental program

2.1 Details of specimens

A total of ten square TSRC specimens were tested to failure, and Fig. 2 shows the details of the specimens. To investigate the slenderness effect on tube confinement, the L/B ratios were chosen as 3 and 6. To realize the concept of TSRC column shown in Fig. 1, the steel tube terminated at 100 mm away from the specimen ends, and the gap height is 10 mm. Stiffeners were disposed at the both tube ends to prevent undesired local failure (see Fig. 2(a)), and the depth and thickness of the stiffeners were 20 mm and 5 mm, respectively.

Details of the test variables for each specimen are provided in Table 1. Two type specimens, with stud shear connectors welding on the *H*-section flanges or without stud shear connectors, were designed to investigate the bond behavior between the concrete and *H*-section, as shown in Fig. 2(c), "The main parameters varied in the tests are length-to-width ratio (L/B = 3, 6) and width-to-thickness ratio of steel tube (B/t = 100, 133), "The details of the specimens are provided in Table 1, where L is the length of the column; B is the outer width of the cross section; t is the thickness of the steel tube; α_t ($\alpha_t = A_t/(A_t+A_s+A_c)$) and α_s ($\alpha_s = A_s/(A_t+A_s+A_c)$) are the steel ratio of the steel tube and

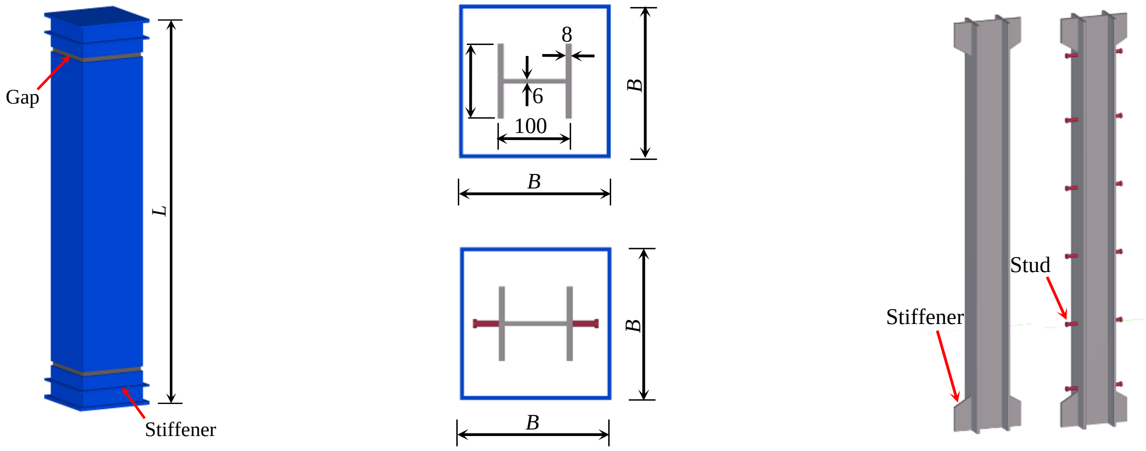

(a) Test specimen (b) Cross-sections (c) Steel sections (inner)

Fig. 2 Details of the specimens

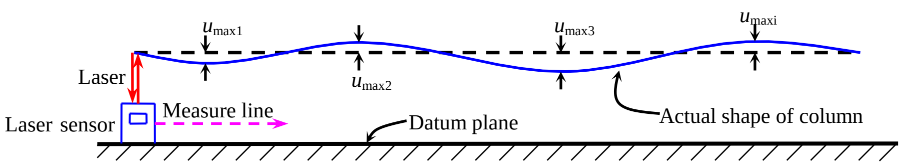

Fig. 3 Measurement of global imperfections

Table 1 Properties and test results of specimens

Specimen	L (mm)	L_e (mm)	B (mm)	t (mm)	$\bar{\lambda}_{EC4}$	$\bar{\lambda}_{AISC}$	Studs	f_{yt} (MPa)	f_{ys} (MPa)	f_{cu} (MPa)	f_{co} (MPa)	E_t (GPa)	E_s (GPa)	E_c (MPa)	α_s	α_t	u_{imp} (mm)	N_{ue} (kN)
S-3-1.5-1	600	445	200	1.5	0.112	0.107	/	324.4	285.4	80.6	61.1	203	205	36483	5.3%	3.0%	/	3277
S-3-1.5-2s	600	445	200	1.5	0.112	0.107	@100	324.4	285.4	80.6	61.1	203	205	36483	5.3%	3.0%	/	3450
S-3-1.5-3s	600	445	200	1.5	0.112	0.107	@100	324.4	285.4	80.6	61.1	203	205	36483	5.3%	3.0%	/	3328
S-6-1.5-1	1200	1300	200	1.5	0.328	0.314	/	324.4	285.4	80.6	61.1	203	205	36483	5.3%	3.0%	4.5	2982
S-6-1.5-2s	1200	1300	200	1.5	0.328	0.314	@200	324.4	285.4	80.6	61.1	203	205	36483	5.3%	3.0%	7.2	2727
S-3-2.0-1	600	445	200	2.0	0.108	0.103	/	290.1	285.4	80.6	61.1	199	205	36483	5.3%	4.0%	/	3496
S-3-2.0-2s	600	445	200	2.0	0.108	0.103	@100	290.1	285.4	80.6	61.1	199	205	36483	5.3%	4.0%	/	3346
S-3-2.0-3s	600	445	200	2.0	0.108	0.103	@100	290.1	285.4	80.6	61.1	199	205	36483	5.3%	4.0%	/	3460
S-6-2.0-1	1200	1300	200	2.0	0.317	0.301	/	290.1	285.4	80.6	61.1	199	205	36483	5.3%	4.0%	6.3	2985
S-6-2.0-2s	1200	1300	200	2.0	0.317	0.301	@200	290.1	285.4	80.6	61.1	199	205	36483	5.3%	4.0%	5.4	3044

*Taking S-3-1.5-2s for example, the first uppercase letter "S" denotes square specimen; the second number "3" represents length-to-width ratio; the third number "1.5" represents thickness of steel tube, mm; the last combination "2s", "2" is the serial number of specimens with same dimensions, and the lowercase letter "s" denotes specimen with stud shear connectors.
L_e: for columns with L/B = 3, $L_e = (L+290)/2$, mm; for columns with L/B = 6, $L_e = L+50\times2$, mm

steel section, respectively; where A_t, A_s, and A_c are the cross-sectional area of the steel tube, steel section, and concrete, respectively. The objective of this study is to investigate the influence of column slenderness, and the corresponding parameters are also presented in Table 1. $\bar{\lambda}_{EC4}$, $\bar{\lambda}_{AISC}$ are the relative slenderness of the column which calculated by Eurocode 4 (2004) and AISC standard (2016), respectively. The cubic strength of concrete (f_{cu}) was determined by the average strength of six 150 mm cubes. In addition, the axial compressive strength of concrete (f_{co}) and the elastic modulus of concrete (E_c) were obtained by testing six 150 mm×150 mm×300 mm prisms. The shear connector stud has a shank diameter and height of 10 mm and 30 mm, respectively. The spacing of the studs for columns with L/B = 3 is 100 mm; for columns with L/B = 6, the spacing is 200 mm. The non-contact laser sensor for displacement measurement was used to monitor the global imperfections of the specimens with L/B = 6 (Fig. 3),

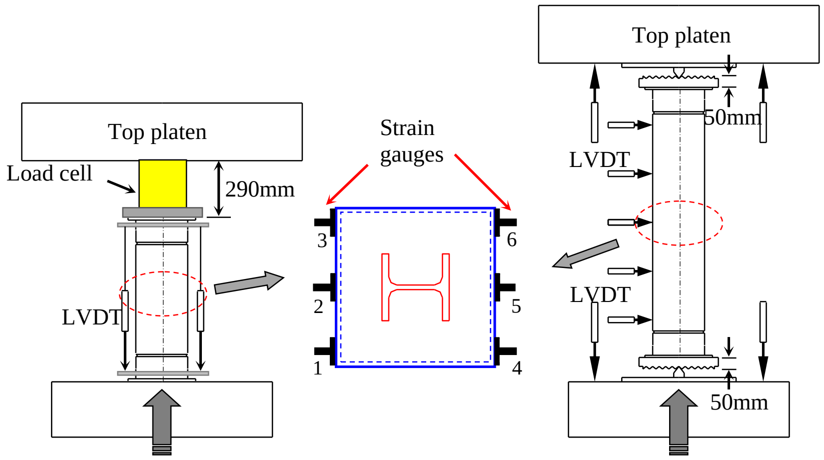

(a) Columns with *L/B* = 3 (b) Strain gauges arrangement (c) Columns with *L/B* = 6

Fig. 4 Schematic view of test set-up and instrumentation layout

and the measurement results, using u_{imp} for simplification, are also summarized in Table 1

$$u_{\text{imp}} = max(|u_{max\,1}|,\ |u_{max\,2}|, \ldots\ |u_{max\,i}|\ldots) \qquad (1)$$

2.2 Test setup and instrumentation layout

All the specimens were performed on a 5000 kN hydraulic compression machine. The test setup and instrument layout are shown in Fig. 4. For the columns with *L/B* = 3, the rigid platens of the compression machine were employed to simulate the fixed boundary conditions. A load cell was arranged on the top of the specimen to monitor the load and to calibrate the measurements of the compression machine. For the columns with *L/B* = 6, two V-shaped edges were employed to ensure the single-curvature bending behavior of the columns. Prior to loading, two plates with thickness of 50mm were assembled at the positions between the V-shape edge and column end plate. Fig. 4 also depicts the instrumentation layout of the tests. For the columns with *L/B* = 3, four linear variable differential transformers (LVDTs) were used to monitor the axial shortening displacement of the specimens. For the columns with *L/B* = 6, five additional LVDTs were arranged along the specimen span with spacing of the column width (*B*) to measure the lateral deflections. Twelve strain gauges were glued onto the tube to measure the axial and transverse strains at the mid-height of the columns, as shown in Fig. 4(b).

3. Experimental results and discussions

3.1 Failure mode and load-deformation relationship

The typical failure modes of columns with *L/B* = 3 are shown in Fig. 5, and the load (*N*) versus axial displacement (*Δ*) curves are presented in Fig. 6. During the initial loading stage, the axial load was approximately proportional to the axial displacement. Tube buckling initially occurred at a load level of about 90% or less of the ultimate strength during the post-peak stage (red dot in Fig. 6), “Concrete crushing can be found at the position where tube buckling occurred by stripping the steel tube from the column. Tube buckling is always a big concern for square CFST columns, especially for columns with thin-walled tubes. A series of

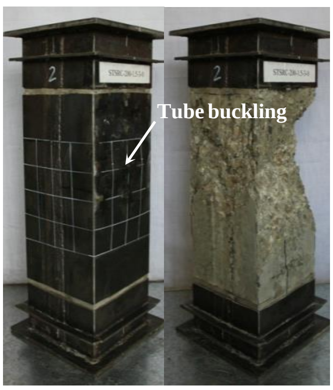

(a) S-3-1.5-1

(b) S-3-2.0-3s

Fig. 5 Failure modes of columns with *L/B* = 3

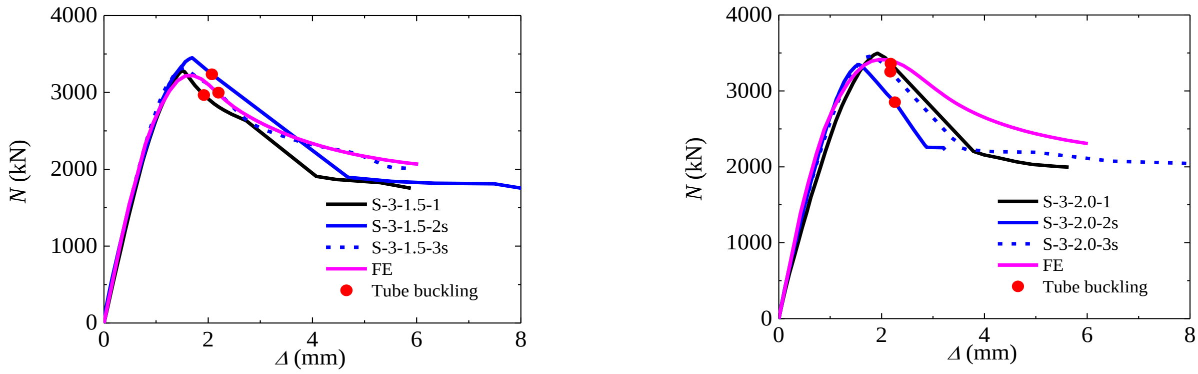

(a) Group t = 1.5 mm (b) Group t =2.0 mm

Fig. 6 Load (N) versus axial displacement (Δ) curves of columns with L/B = 3

(a) S-6-1.5-2s (b) S-6-2.0-2s

Fig. 7 Failure modes of columns with L/B = 6

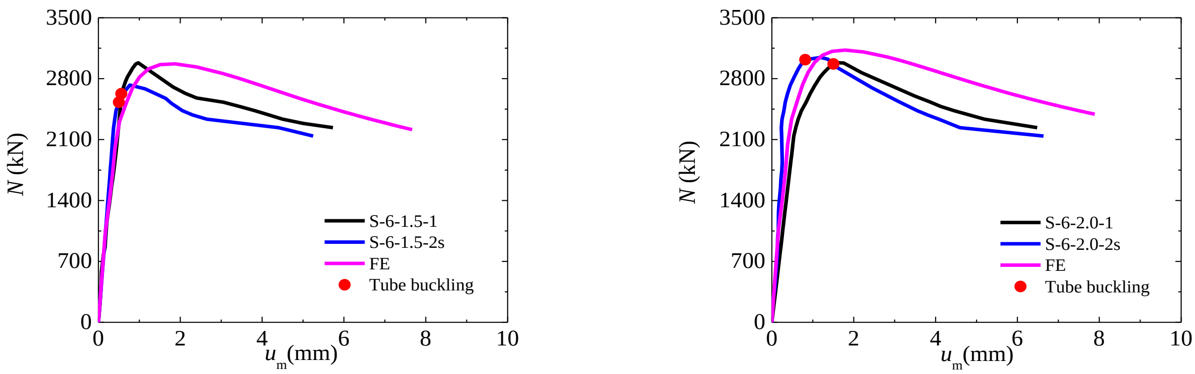

(a) Group t = 1.5 mm (b) Group t =2.0 mm

Fig. 6 Load (N) versus axial displacement (Δ) curves of columns with L/B = 3

tests about thin-walled CFST columns (B/t = 76, 100) were conducted by Tao *et al*. (2007, 2009), the test results indicated that the steel tube buckled when the load attained 30%-40% of the maximum load in the pre-peak stage. However, for square TSRC columns, the tube buckling was effectively delayed since axial load was not directly applied on the steel tube, so the tube can provide more effective confinement to the concrete core.

In contrast, the failure modes of columns with L/B = 6 are shown in Fig. 7. Tube buckling was observed near the column ends due to the end effects, and concrete crushing can be found at the locations where tube buckling developed. Fig. 8 presents the axial load (N) versus lateral deflection (u_m) at mid-span curves. Compared to the short specimens, tube buckling of the specimens with L/B = 6 occurred earlier due to the larger slenderness ratio. As a matter of fact, buckling of the outer tube initially occurred at a load level of 88%-94% of the maximum load for specimens with tube thickness of 1.5mm, while occurred generally at the peak load point for those with tube thickness of 2.0 mm.

The effects of stud shear connectors were also investigated, and the results indicated that studs had no significant influences on the failure mode, ultimate strength, and ductility for all the columns. This result may be explained as follows: for the columns subjected to monotonically compressive loads, the shear-sliding deformation of between the concrete and steel section was very small during the tests, thus the studs could not be utilized, which further resulted in no significant influences on the performance of the columns. However, the studs would play an important role when the columns subjected to seismic loading.

3.2 Elastic-plastic analysis of steel tube

The elastic-plastic analysis method (Zhang *et al*. 2005) was employed to convert the measured strains into stresses. Typical load-tube stress responses of the columns are shown in Fig. 9, in which σ_v and σ_h are the longitudinal stress and transverse stress of the steel tube, respectively. σ_z is the equivalent stress which determined by the following equation

$$\sigma_z = \frac{\sqrt{2}}{2}\sqrt{(\sigma_v - \sigma_h)^2 + \sigma_v^2 + \sigma_h^2} \tag{2}$$

In the elastic stage, the stress-strain relationship is

$$\begin{bmatrix}\sigma_h \\ \sigma_v\end{bmatrix} = \frac{E_s}{1-\mu_s^2}\begin{bmatrix}1 & \mu_s \\ \mu_s & 1\end{bmatrix}\begin{bmatrix}\varepsilon_h \\ \varepsilon_v\end{bmatrix} \tag{3}$$

In the elastic-plastic stage, the stress-strain equations are based on the increment theory

$$d\sigma_h = \frac{E_s^t}{1-\mu_{sp}^2}\left(d\varepsilon_h + \mu_{sp} d\varepsilon_v\right) \tag{4a}$$

$$d\sigma_v = \frac{E_s^t}{1-\mu_{sp}^2}\left(d\varepsilon_v + \mu_{sp} d\varepsilon_h\right) \tag{4b}$$

In the plastic hardening stage, von Mises yield criterion and Prandtl-Reuss flow rule are adopted to analyze the behavior of steel

$$d\sigma_h = \frac{E_s^p}{Q}\left[(\sigma_v + 2p)d\varepsilon_h + \left(-\sigma_v\sigma_h + 2\mu_s^p p\right)d\varepsilon_v\right] \tag{5a}$$

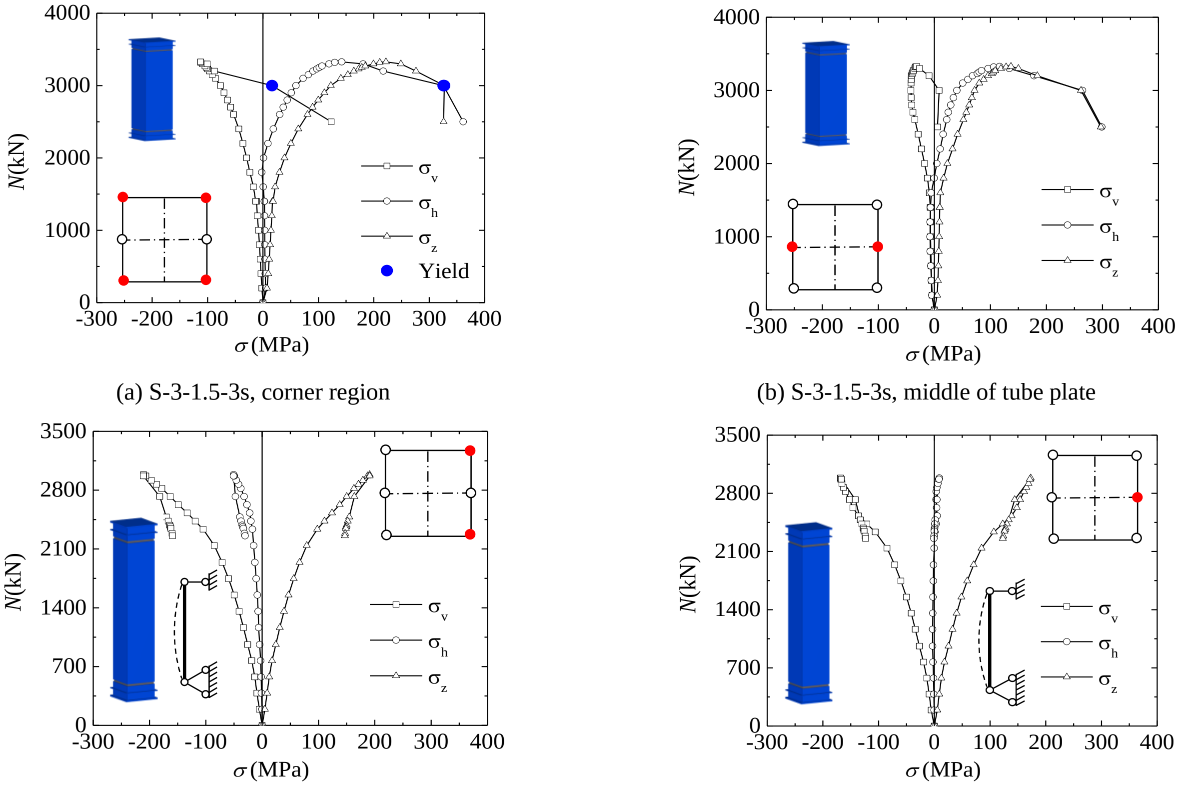

(a) S-3-1.5-3s, corner region

(b) S-3-1.5-3s, middle of tube plate

(c) S-6-2.0-1, corner region

(d) S-6-2.0-1, middle of tube plate

Fig. 9 Load-tube stress responses of columns

$$d\sigma_v = \frac{E_s^p}{Q}\left[(\sigma_h + 2p)d\varepsilon_v + \left(-\sigma_h\sigma_v + 2\mu_s^p p\right)d\varepsilon_h\right] \quad (5b)$$

where μ_{sp} is the Poisson's ratio in the elastic-plastic stage; E_s^p and μ_s^p are the tangent modulus and the Poisson's ratio in the plastic hardening range, respectively.

The load-tube stress response of specimen S-3-1.5-3s is selected to illustrate the stress development of short columns. The corner region of the tube did not yield until the applied load declined at a load level of about 90% of the maximum load (Fig. 9(a)), "Considering the results of failure modes, it can be concluded that the yielding of steel tube was due to the concrete crushing and the subsequent tube buckling during the post-peak stage. At the peak load point, the transverse stress (σ_h) of tube in corner region was higher than that at middle of the steel plate, indicating that the concrete core was better confined in the corner region (Fig. 9(b)).

In contrast to short columns, the tube stress analysis of columns with L/B = 6 was also conducted (Figs. 9(c)-(d)), "Since concrete crushing occurred at the location near the column ends, the tube strains in mid-span of the column should be lower than the strains in the anticipating situation that concrete crushing occurred at the mid-span of the column. The stresses of the tube at the middle of the column were less than the yield strength during the tests, so in a qualitative perspective only, the tendency of tube confinement is discussed here. The tendency of the deflection is also shown in Figs. 9(c)-(d), "Due to the lateral deflection, the compressive stress of the column cross-section showed a gradient distribution, and only the tube at the most compressed region is discussed here. Due to the corner confinement effect of square tube, the stress of tube in corner region was slightly higher than that in middle of the steel plate at the same load level. Compared to the results of short columns (L/B = 3) (Figs. 9(a)-(b)), obvious longitudinal stress (σ_v) existed in the tube of columns with L/B = 6 due to the longer length between the interface of concrete and tube, which indicated that the friction and bond between concrete could no longer be ignored. In general, the axial load carried by square tube due to friction and bond increased with the increase of L/B ratios, while the confinement effect of tube was just the opposite.

4. Finite element analysis

4.1 Material properties

ABAQUS (2012) was employed to simulate the behavior of square TSRC columns. An elastic-plastic model with five stages was used to describe the mechanical behavior of mild steel (Fig. 10(a)), and the details of the stress-strain equations can be found in Han's monograph (2016), "For the high strength steel (> 420 MPa), the bi-linear model was adopted, and the stress-strain relationship is shown as Fig. 10(b).

The damage plasticity model was used in the analysis of concrete. For the TSRC column, the strength and plasticity of core concrete increased since the core concrete was subjected to triaxial loading due to the tube confinement. In the finite element (FE) model, one of the key respects is to confirm an equivalent stress-strain relationship which

(a) Mild steel (b) High strength steel

Fig. 10 Stress-strain model of steel

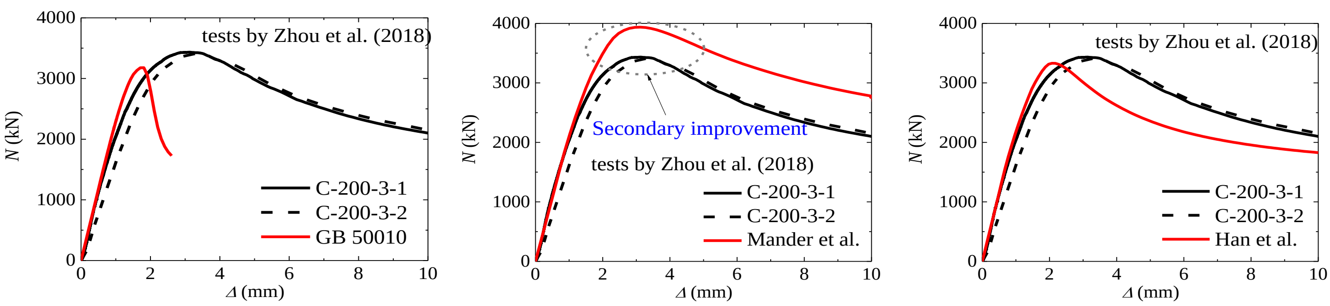

(a) Plain concrete model (b) Mander's model (c) Han's model

Fig. 11 Comparision of FE results and test results suitable for concrete of tubed columns. The strength improvement of concrete can be achieved by adjusting the yielding surface of the material (Lubliner *et al*. 1989), and the adjustment can be automatically achieved by the software through the calculation of the confining stress. However, the plastic behavior cannot be accurately described by using the stress-strain relationship of plain concrete (GB 50010 2010), "Fig. 11(a) shows the comparison of the FE results using the stress-strain relationship of plain concrete and the test results on the axial load behavior of circular TRC columns (Zhou *et al*. 2018), "For the confined concrete, the strain of the maximum stress would increase, and the descending branch of the stress-strain curve would tend to become even. Therefore, the FE results in Fig. 11(a) show distinguishable difference with the test results. For the stress-strain relationship of confined without modification (Mander *et al*. 1988), the strength improvement of confined concrete is already considered in the relationship. When the stress-strain relationship was used in FE analysis, the software still takes the confining stress into consideration, resulting in "secondary improvement" (Fig. 11(b)), "Therefore, it is necessary to make some modifications on the stress-strain relationships of actual concrete in the FE calculations.

An equivalent stress-strain model of concrete for FE analysis was proposed by Han (2016) to solve the above contradictions. In the model, the strain of the maximum stress $\varepsilon_{\mathrm{FE}}$ is enlarged by an additional coefficient according to a large amount of trial calculations (Eq. (6)), and the maximum stress of the stress-strain model is equal to the axial compressive strength of unconfined concrete f_{co}. The feasibility of Han's model has been verified by various performance tests of CFST columns, which demonstrates that this approach is efficient and feasible. The confinement on concrete of TRC short columns is more pronounced compared to that of CFST columns, thus Han's model is not applicable for TRC columns, as shown in Fig. 11(c).

$$\varepsilon_{\mathrm{FE}} = \varepsilon_{\mathrm{co}} + 800\xi^{0.2} \times 10^{-6} \tag{6}$$

where $\varepsilon_{\mathrm{co}}$ is the peak strain of unconfined concrete; ξ is the confinement factor of CFST columns.

Following the approach of Han's model, a new equivalent stress-strain model was proposed by modifying Mander's model through a large amount of tentative calculations. Fig. 12 shows the equivalent stress-strain curves for both unconfined concrete (f_l = 0 MPa) and confined concrete (f_l = 0.5 MPa for instance), "As can be seen, the strain of the maximum stress increases with the increase in the effective confining stress (f_l), and the descending branch tends to become even due to the confinement. The new equivalent stress-strain relationship, which is suitable for the FE model in ABAQUS software, is shown as following

$$f = \frac{f_{\mathrm{co}} x r}{r - 1 + x^{r}} \tag{7a}$$

where

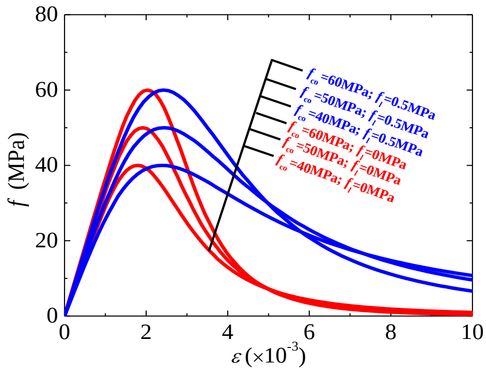

Fig. 12 Proposed equivalent stress-strain curves of concrete

$$x = \varepsilon / \varepsilon_{\mathrm{FE}} \tag{7b}$$

$$\varepsilon_{\mathrm{FE}} = \varepsilon_{\mathrm{cc}} - \left(\frac{f_{\mathrm{cc}}}{f_{\mathrm{co}}} - 1\right)\varepsilon_{\mathrm{co}} \tag{7c}$$

$$\varepsilon_{\mathrm{cc}} = \left[1 + 5\left(\frac{f_{\mathrm{cc}}}{f_{\mathrm{co}}} - 1\right)\right]\varepsilon_{\mathrm{co}} \tag{7d}$$

$$\varepsilon_{\mathrm{co}} = (1300 + 12.5 f_{\mathrm{co}}) \times 10^{-6} \tag{7e}$$

$$r = \frac{E_c}{E_c - E_{sec}} \tag{7f}$$

$$E_c = 4730\sqrt{f_{\mathrm{co}}} \tag{7g}$$

$$E\mathrm{cc}_{\mathrm{cc}_{sec}} \tag{7h}$$

$$f_{\mathrm{cc}} = f_{\mathrm{co}}\left(-1.254 + 2.254\sqrt{1 + 7.94\frac{f_l}{f_{\mathrm{co}}}} - 2\frac{f_l}{f_{\mathrm{co}}}\right) \tag{7i}$$

4.2 Element type, interface and boundary conditions

The FE model considers the steel tube and the encased steel section as 4-noded fully integrated shell element (S4), and considers the concrete as 8-noded solid element with reduced integration (C3D8R), "A surface-based interaction with a contact pressure model in the normal direction, and with a Coulomb friction model in the tangential direction, was used to simulate the interface between the steel tube and the core concrete. The friction coefficient of the interface model was chosen as 0.6. An average bond stress of 0.6 MPa was used in the Coulomb friction model. As aforementioned, the test results indicated that the studs had no significant influence on the mechanical behavior of the specimens, thus the studs were not considered in the FE model. Moreover, the embedded element technique was used to model the interaction between encased steel section and core concrete. The columns were loaded through the pin-lines in the FE models to in accordance with the testing procedure, as shown in Fig. 13.

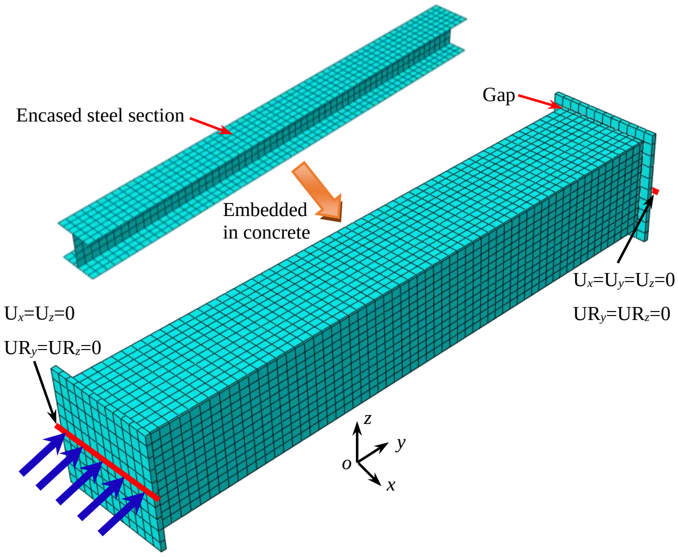

Fig. 13 Typical FE model

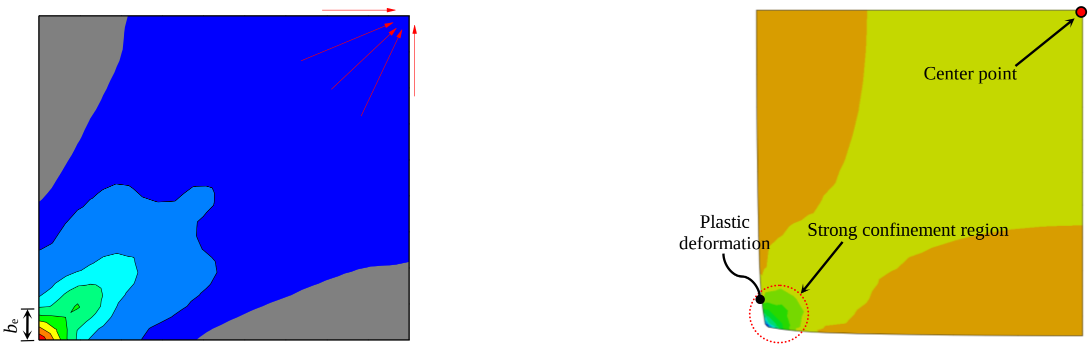

(a) Confining stress (b) Longitudinal stress

Fig. 14 Stress distribution of concrete

4.3 Confinement model

The concrete in corner region of square TSRC column would suffer stronger confinement due to the plastic deformation of concrete, and a quarter-column model (L/B = 3) was precisely modeled to investigate the corner effect. Fig. 14 shows the distribution of confining stress and longitudinal stress of concrete at the peak load point, respectively. The corner of square cross section shows higher confining pressures (Fig. 14(a)), and the longitudinal stress of concrete shows a similar tendency due to the confinement effect (Fig. 14(b)), "Here we define the region where the longitudinal stress is higher than that of center point as "strong confinement region", and the width of the strong confinement region is named as effective width "b_e". Apparently, the effective width b_e is influenced by width-to-thickness ratio of steel tube. Fig. 15 shows the FE analysis results, and β denotes the effective width (b_e) to the width of concrete (B-2t) ratio. A regression equation was proposed for the calculation of β based on the FE results

$$\beta = \frac{b_e}{B-2t} = 0.214e^{\frac{-(B/t-2)}{28.6}} + 0.038 \quad (30 \leq B/t \leq 150) \tag{8}$$

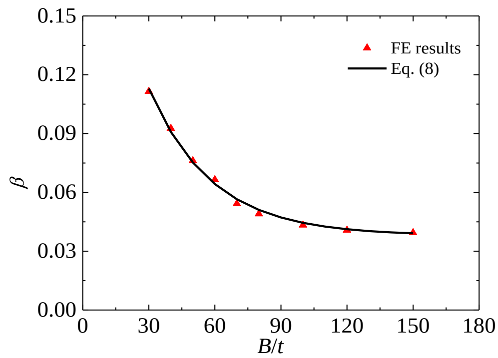

Fig. 15 FE results of β

To account for the corner effect, a confinement effectiveness coefficient k_e is introduced to relate the confined concrete area A_e and the total area of concrete A_c. The confined area A_e is assumed to occur within the region where the arching action has been fully developed, and the arching action is represented in the form of a second degree parabola with an initial tangent slope of 45°, as shown in Fig. 16, and k_e can be obtained by Eq. (9), "It should be noted that the steel section in unconfined regions has been

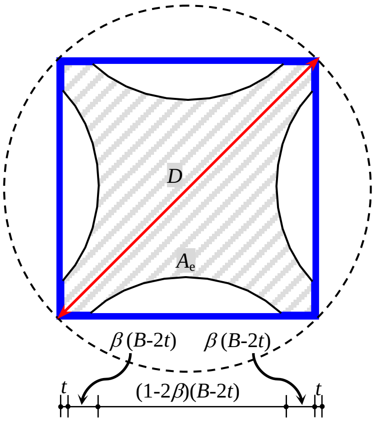

Fig. 16 Effectively confined concrete area

double counted. However, the influence of the simplification is slight and the final results are conservative.

$$k_e = \frac{A_e}{A_c} = \frac{1 - \frac{2}{3}(1 - 2\beta)^2 - \alpha_s}{1 - \alpha_s} \tag{9}$$

In Eq. (7), the effective confining stress of steel tube f_l is

$$f_l = k_e f_l' \tag{10}$$

where f_l' is the confining stress of the equivalent circular section, and can be calculated as

$$f_l' = 2tf_h/(D - 2t) \tag{11}$$

where f_h is the average hoop stress of the equivalent circular section. The tests which conducted by Zhou *et al*. (2018) indicated that the confinement of tube decreased with the increase in length-to-width/diameter ratio of the column, and the average hoop stress f_h can be calculated as follows

$$f_h = \frac{f_{yt}}{0.2 \times (L_t/D)^{1.5} + 1} \tag{12}$$

where L_t is the length of the steel tube, and L_t = L-200 mm in this paper.

4.4 Geometric imperfections and model verification

The geometric imperfections of square tubed SRC column include the global imperfection of column and the local imperfection of thin-walled steel tube. The local geometric imperfection shape of steel tube was often assumed as a magnitude of the lowest buckling mode or eigenmode. For square tubed SRC column, the core concrete provides a rigid support for the steel tube, thus the imperfection shape of tube can be assumed as the buckling mode which shown in Fig. 17. The expression of the shape in Fig. 17 can be assumed as the cosine form as Eq. (13), where ω_0 is the magnitude of the imperfection. The effects of the local imperfections of steel tube were analyzed by Tao *et al*. (2009) and Zhou *et al*. (2015), and the results

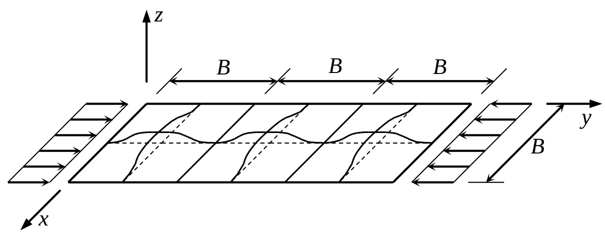

Fig. 17 Assumed local imperfections of thin-walled tube for CFST columns

showed that local imperfections of steel tube induced only a slight strength reduction since most of strength of the column is contributed by its SRC core.

There are two main approaches, namely initial out-of-straightness or initial eccentricity, to take the global imperfections of column into consideration. The effects of two approaches were analyzed by Ellobody *et al*. (2011), and it was found that initial out-of-straightness and initial eccentricity have a similar effect on the column strength. Therefore, it is reasonable to take the alternative factor (initial out-of-straightness or initial eccentricity) as the global imperfection for FE analysis.

Based on the analysis above, the column with only initial eccentricity was adopted for further parametric analysis in this paper, and the global imperfection amplitude was chosen as L/200 according to a large amount of trial calculations. As can be seen from Figs. 6 and 8, good agreements are observed between the predicted results and test results.

$$\omega = \frac{\omega_0}{4}\left(1 - cos\frac{2\pi x}{B}\right)\left(1 - cos\frac{2(L/B)\pi y}{L}\right) \tag{13}$$

4.5 Parametric analysis

The influences of steel yield strength (f_{yt} and f_{ys}), concrete strength (f_{co}) and width-to-thickness ratio of steel tube (B/t) are analyzed through FE models, and the results are shown in Fig. 18. The basic calculating conditions of the columns in Fig. 16 are B = 600 mm, f_{yt} = f_{ys} = 300 MPa, f_{co} = 60 MPa.

Fig. 18(a) shows the N versus L/B ratio curves of columns with different steel yield strengths. Generally, the curves can be divided into three stages. When L/B ratio is less than or equal to 4, the column fails by steel yielding and concrete crushing. With the increase in L/B ratio, the failure of the column changes from concrete crushing to elastoplastic buckling, and the differences among the values of ultimate strengths with different steel yield strengths decrease with the increasing L/B ratio. When L/B ratio is greater than 34, the column fails by elastic buckling, thus the columns with different steel strengths exhibit same values. Fig. 18(c) shows the size sensitivity of the columns, and $N_{(3)}$ in the Fig. represents the ultimate strength of the column with L/B = 3. As can be seen, the dimension size only has moderate influence on the strength ratio $N/N_{(3)}$. In general, the curves show two different tendencies due to the different failure modes.

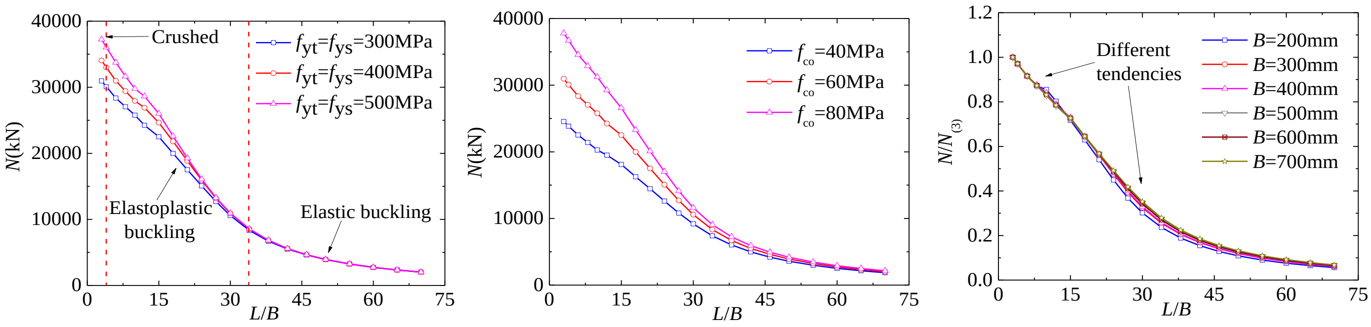

(a) Steel yield strength (b) Concrete strength (c) Section dimension

Fig. 18 Parametric analysis results

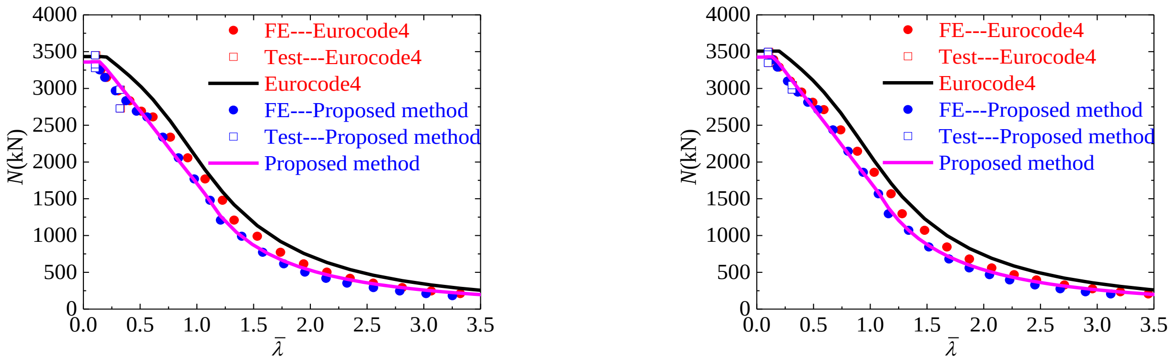

(a) Group t = 1.5 mm (b) Group t = 2.0 mm

Fig. 19 Comparison of FE results and EC4 predictions

5. Current design method

Up to now, there is no design code or specification for the calculation of square TSRC column. Considering that this kind of composite column is so close to CFST column, the calculating methods for CFST column will be used for reference to predict the ultimate strength of TSRC column under axial compression.

5.1 Eurocode 4

According to EC4 (2004), the ultimate strength of composite columns under axial load can be calculated by Eq. (14), "The ultimate strengths obtained from the FE models are compared with the unfactored design strengths N_u^{EC4}, as shown in Fig. 19. The global imperfection amplitude of L/200 was recommended in EC4 for square steel tubular column filled with steel reinforced-concrete, and the same amplitude was adopted in the FE analysis. As can be seen, the EC4 predictions are unconservative compared with the FE results.

$$N_u^{\mathrm{EC4}} = \varphi N_{\mathrm{pl,Rd}} \tag{14}$$

where

$\varphi -$ reduction factor

$$\varphi = \frac{1}{\Phi + \sqrt{\Phi^2 - \bar{\lambda}^2}}, \quad \text{but} \quad \varphi \leq 1.0$$

$$\Phi = 0.5\left[1 + 0.34(\bar{\lambda} - 0.2) + \bar{\lambda}^2\right]$$

$$N_{\mathrm{pl,Rd}} = A_t f_{\mathrm{yt}} + A_c f_{\mathrm{co}} + A_s f_{\mathrm{ys}}$$

$\bar{\lambda} -$ relative slenderness

$$\bar{\lambda} = \sqrt{\frac{N_{\mathrm{pl,Rd}}}{N_{\mathrm{cr}}}}$$

$$N_{\mathrm{cr}} = \frac{\pi^2 (EI)_{\mathrm{eff}}}{L_e^2}$$

$$(EI)_{\mathrm{eff}} = E_t I_t + E_s I_s + 0.6 E_c I_c$$

5.2 AISC Standard

According to AISC standard (2016), the ultimate strength of composite columns under axial compression can be calculated by Eq. (15), "The ultimate strengths obtained from the FE results are compared with the unfactored design strengths N_u^{AISC}, as shown in Fig. 20. For short columns, the AISC predictions are slightly conservative compared to FE results due to the underestimation of tube confinement on the core concrete. Similar to the comparison of EC4 predictions and FE results, the AISC predictions are unconservative for the slender columns.

when, $P_e \geq 0.44 P_o$

$$N_u^{\mathrm{AISC}} = P_o \left[0.658^{\left(\frac{P_o}{P_e}\right)}\right] \tag{15a}$$

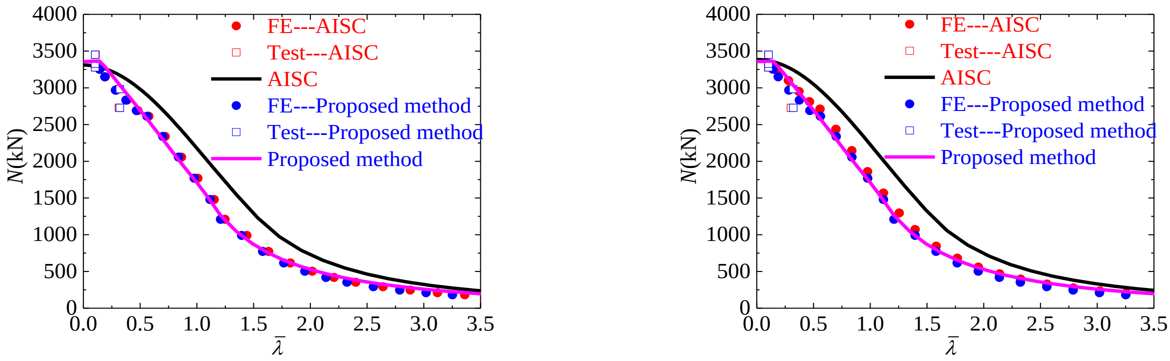

(a) Group t = 1.5 mm (b) Group t = 2.0 mm

Fig. 20 Comparison of FE results and AISC predictions

when, $P_e < 0.44P_o$

$$N_u^{\mathrm{AISC}} = 0.877P_e \tag{15b}$$

where

$$P_o = A_t f_{\mathrm{yt}} + 0.95A_c f_{\mathrm{co}} + A_s f_{\mathrm{ys}}$$

$$P_e = \frac{\pi^2 (EI)_{\mathrm{eff}}}{L_e^2}$$

$$(EI)_{\mathrm{eff}} = E_t I_t + E_s I_s + C_3 E_c I_c$$

$$C_3 = 0.6 + 2\left(\frac{A_t}{A_c + A_t}\right) \leq 0.9$$

6. Proposed method

Based on the comparisons of current specification predictions and FE results, it can be concluded that the current design methods are not suitable for square TSRC columns. Therefore, it is necessary to propose a new approach to predict the axial strength of this composite column.

The influences of the steel tube on the resistance of TSRC column can be mainly divided into two respects: direct resistance and tube confinement on concrete. In the proposed method, the strength of square TSRC cross-section (N_0) is considered to be the sum of three parts, namely the equivalent strength of steel tube, the strength of confined concrete, and the strength of steel section:

$$N_0 = \alpha A_t f_v + A_c f_{\mathrm{cc}} + A_s f_{\mathrm{ys}} \tag{16}$$

where α is the shape coefficient of square tube; A_t, A_c, and A_s are the cross-sectional area of steel tube, concrete, and steel section, respectively.

The tube in corner region can be considered as yielding when calculating the ultimate strength, and the longitudinal stress (f_v) can be determined by Eq. (17) according to von Mises yield criterion

$$f_v = \left(\sqrt{4f_{\mathrm{yt}}^2 - 3f_h^2} - f_h\right)/2 \tag{17}$$

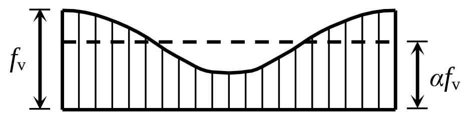

Fig. 21 The shape coefficient of square tube

For square TSRC column, the distribution of longitudinal stress along the tube width is non-uniform, the longitudinal stress of tube in corner region is higher than that in middle region, as shown in Fig. 21. A shape coefficient α is used to estimate the average longitudinal stress, and it is greatly influenced by B/t ratio. However, for square TSRC column, the majority of load is resisted by concrete core and steel section, thus the equivalent strength of steel tube is relatively small. Therefore, the shape coefficient α is arbitrarily taken as 0.5 in this paper for simplification.

When the influence of L/B ratio is considered, the ultimate strength of square TSRC column can be calculated by the following equation

$$N_u = \varphi N_0 \tag{18}$$

Fig. 22 shows the statistical results of tests and FE models. According to the results, the stability coefficient φ can be calculated by Eq. (19), "It should be noted that for a given cross-section, the ultimate strengths of critical sections of columns with different slenderness ratios are different due to the different tube confinement, and this is a key characteristic to separate TSRC column from other composite columns.

when: $\bar{\lambda} \leq 0.15$

$$\varphi = 1 \tag{19a}$$

when: $0.15 \leq \bar{\lambda} \leq 1.0$

$$\varphi = \frac{\left[1 + \frac{(0.499\bar{\lambda}+0.926)}{\bar{\lambda}^2}\right]}{2} - \sqrt{\left[1 + (0.499\bar{\lambda} + 0.926)/\bar{\lambda}^2\right]^2/4 - 1/\bar{\lambda}^2} \tag{19b}$$

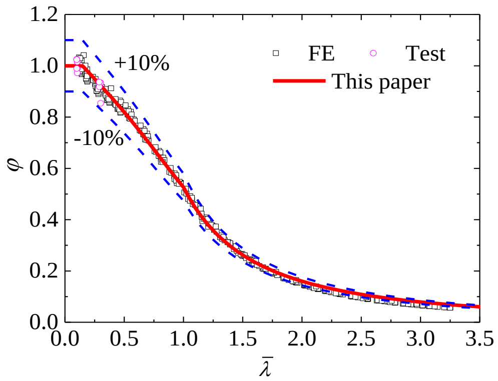

Fig. 22 Comparison of predictions obtained from proposed method with test and FE results

when: $\bar{\lambda} \geq 1.0$

$$\varphi = \frac{\left[1 + \frac{(1.461\bar{\lambda} - 0.036)}{\bar{\lambda}^2}\right]}{2} - \sqrt{\left[1 + (1.461\bar{\lambda} - 0.036)/\bar{\lambda}^2\right]^2 /4 - 1/\bar{\lambda}^2} \quad (19c)$$

where

$$\bar{\lambda} = \sqrt{\frac{N_0}{N_{cr}}};$$

$$N_{cr} = \frac{\pi^2 (EI)_{eff}}{L_e^2};$$

$$(EI)_{eff} = E_t I_t + E_s I_s + C E_c I_c;$$

$$C = 0.6 + 2\left(\frac{A_t + A_s}{A_c + A_t + A_s}\right) \leq 0.9$$

7. Conclusions

This paper presented experimental investigation and nonlinear analysis on the axial load behavior of square TSRC columns. Ten columns were tested to investigate the effects of length-to-width ratio (L/B) of the specimens, width-to-thickness ratio (B/t) of the steel tubes, and use of stud shear connectors on the steel sections. The following conclusions were drawn from the study:

- Tube buckling of square TSRC column was effectively delayed since axial load was not directly applied on the steel tube. For the columns subjected to monotonically compressive load, stud shear connectors were found to have no influence on the failure mode, ultimate strength, and ductility of the specimens.
- The transverse stress of tube in corner region was higher than that at middle of the steel plate, thus the concrete in corner region was better confined. The axial load carried by square tube due to friction and bond increased with the increase in L/B ratio, while the confinement effect of tube was just the opposite.
- Following the approach of Han's model, an equivalent stress-strain model for confined concrete in FE analysis was proposed by modifying Mander's model, and a new confinement model for square TSRC column was proposed according to the FE results.
- The design methods specified in Eurocode 4 and the AISC standard were used to predict the ultimate strength of the innovative columns. The comparisons indicated that the predictions of Eurocode4 and the AISC standard were unconservative for the slender columns.
- A method for calculating the ultimate strength of square TSRC column was proposed, in which the slenderness effect on the tube confinement was considered.

Acknowledgments

The research work reported herein was made possible by the National Natural Science Foundation of China (nos. 51438001, 51878097, and 51908045), and the Fundamental Research Funds for the Central Universities (nos. 300102219109 and 300102219310). The financial supports are highly appreciated.

References

AISC 360 (2016), Specification for structural steel buildings, American Institute of Steel Construction; Chicago, IL, USA.

Chen, Z., Liu, X. and Zhou, W. (2018), "Residual bond behavior of high strength concrete-filled square steel tube after elevated temperatures", *Steel Compos. Struct., Int. J.*, **27**(4), 509-523. https://doi.org/10.12989/scs.2018.27.4.509

Ellobody, E., Young, B. and Lam, D. (2011), "Eccentrically loaded concrete encased steel composite columns", *Thin-Wall. Struct.*, **49**(1), 53-65. https://doi.org/10.1016/j.tws.2010.08.006

Eurocode 4 (2004), Design of composite steel and concrete structures. Part 1.1: General rules and rules for buildings, European Committee for Standardization; Brussels, Belgium.

Gardner, N.J. and Jacobson, E.R. (1967), "Structural behavior of concrete filled steel tubes", *ACI J. Proceedings*, **64**(7), 404-413.

GB 50010 (2010), Code for design of concrete structures, Ministry of Housing and Urban-Rural Development of China; Beijing, China. [In Chinese]

Han, L.H. (2016), *Concrete Filled Steel Tubular Columns-Theory and Practice*, (7th Edition), Science Press, Beijing, China. [In Chinese]

Keo, P., Somja, H., Nguyen, Q.H. and Hjiaj, M. (2015), "Simplified design method for slender hybrid columns", *J. Constr. Steel Res.*, **110**, 101-120. https://doi.org/10.1016/j.jcsr.2015.03.006

Kim, C.S., Park, H.G., Chung, K.S. and Choi, I.R. (2011), "Eccentric axial load testing for concrete-encased steel columns using 800 MPa steel and 100 MPa concrete", *J. Struct. Eng.*, **138**(8), 1019-1031. https://doi.org/10.1061/(ASCE)ST.1943-541X.0000533

Ky, V.S., Tangaramvong, S. and Thepchatri, T. (2015), "Inelastic analysis for the post-collapse behavior of concrete encased steel composite columns under axial compression", *Steel Compos. Struct., Int. J.*, **19**(5), 1237-1258. https://doi.org/10.12989/scs.2015.19.5.1237

Liu, Y., Xiong, Z., Feng, Y. and Jiang, L. (2017), "Concrete-filled rectangular hollow section X joint with Perfobond Leister rib structural performance study: Ultimate and fatigue experimental Investigation", *Steel Compos. Struct., Int. J.*, **24**(4), 455-465. https://doi.org/10.12989/scs.2017.24.4.455

Lubliner, J., Oliver, J., Oller, S. and Onate, E. (1989), "A plastic-damage model for concrete", *Int. J. Solids Struct.*, **25**(3), 299-326. https://doi.org/10.1016/0020-7683(89)90050-4

Mander, J.B., Priestley, M.J. and Park, R. (1988), "Theoretical stress-strain model for confined concrete", *J. Struct. Eng.*, **114**(8), 1804-1826. https://doi.org/10.1061/(ASCE)0733-9445(1988)114:8(1804)

Qi, H., Guo, L., Liu, J., Gan, D. and Zhang, S. (2011), "Axial load behavior and strength of tubed steel reinforced-concrete (SRC) stub columns", *Thin-Wall. Struct.*, **49**(9), 1141-1150. https://doi.org/10.1016/j.tws.2011.04.006

Systèmes, D. (2012), ABAQUS Analysis User's Manual, Version 6.12. Dassault Systèmes, Providence, RI, USA.

Tao, Z., Han, L.H. and Wang, D.Y. (2007), "Experimental behavior of concrete-filled stiffened thin-walled steel tubular columns", *Thin-Wall. Struct.*, **45**(5), 517-527. https://doi.org/10.1016/j.tws.2007.04.003

Tao, Z., Uy, B., Han, L.H. and Wang, Z.B. (2009), "Analysis and design of concrete-filled stiffened thin-walled steel tubular columns under axial compression", *Thin-Wall Struct.*, **47**(12), 1544-1556. https://doi.org/10.1016/j.tws.2009.05.006

Tomii, M., Sakino, K., Xiao, Y. and Watanabe, K. (1985), "Earthquake resisting hysteretic behavior of reinforced concrete short columns confined by steel tube", *Proceedings of the International Speciality Conference on Concrete Filled Steel Tubular Structures*, Harbin, China, August.

Wang, X., Liu, J. and Zhou, X. (2016), "Behavior and design method of short square tubed-steel-reinforced-concrete columns under eccentric loading", *J. Constr. Steel Res.*, **116**, 193-203. https://doi.org/10.1016/j.jcsr.2015.09.018

Zhang, S., Guo, L., Ye, Z. and Wang, Y. (2005), "Behavior of steel tube and confined high strength concrete for concrete-filled RHS tubes", *Adv. Struct. Eng.*, **8**(2), 101-116. https://doi.org/10.1260/1369433054037976

Zhou, X. and Liu, J. (2010), "Seismic behavior and strength of tubed steel reinforced concrete (SRC) short columns", *J. Constr. Steel Res.*, **66**(7), 885-896. https://doi.org/10.1016/j.jcsr.2010.01.020

Zhou, X.H., Yan, B. and Liu, J.P. (2015), "Behavior of square tubed steel reinforced-concrete (SRC) columns under eccentric compression", *Thin-Wall. Struct.*, **91**, 129-138. https://doi.org/10.1016/j.tws.2015.01.022

Zhou, X.H., Yan, B., Liu, J.P. and Gan, D. (2018), "Axial load behavior of circular tubed reinforced concrete with different length-to-diameter ratios", *J. Build. Struct.*, **39**(12), 11-21. [In Chinese]

Zhu, W., Jia, J. and Zhang, J. (2017), "Experimental research on seismic behavior of steel reinforced high-strength concrete short columns", *Steel Compos. Struct., Int. J.*, **25**(5), 603-615. https://doi.org/10.12989/scs.2017.25.5.603

BU